

pubs.acs.org/journal/apchd5 Article

## **Lattice Resonances for Thermoplasmonics**

Lauren Zundel, Kellen Malone, Luis Cerdán, Rosario Martínez-Herrero, and Alejandro Manjavacas\*



Cite This: ACS Photonics 2023, 10, 274-282



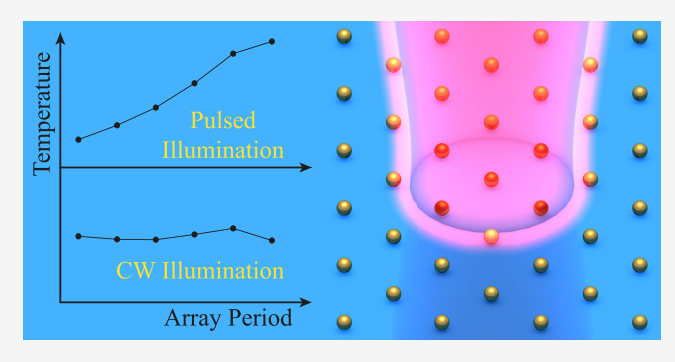
**ACCESS** 

Metrics & More

Article Recommendations

Supporting Information

ABSTRACT: Thanks to their ability to support localized surface plasmons, metallic nanostructures have emerged as ideal tools to transduce light into heat at the nanoscale, giving birth to the field of thermoplasmonics. When arranged in a periodic array, the localized plasmons of metallic nanostructures can interact coherently to generate a collective mode known as a lattice resonance. This collective mode, whose wavelength is controlled by the periodicity of the array, produces a stronger and more spectrally narrow optical response than that of the localized plasmons supported by the individual nanostructures. Motivated by the exceptional properties of the lattice resonances of periodic arrays of metallic nanoparticles, here, we investigate their use for



applications in thermoplasmonics. Through a comprehensive analysis based on a coupled dipole model, we show that arrays supporting a lattice resonance absorb more energy per nanoparticle, and thus achieve a much larger increase in temperature under pulsed illumination conditions, than those that do not support such a mode. On the contrary, for continuous wave illumination conditions, we find that the temperature increase is mostly independent of the array period for the systems under consideration. Furthermore, by analyzing arrays with two nanoparticles per unit cell, we show that it is possible to engineer their lattice resonances to selectively absorb light in one of the nanoparticles without exciting the other. The results of this work pave the way for the development of thermoplasmonics applications exploiting the exceptional optical response and tunability provided by lattice resonances.

KEYWORDS: thermoplasmonics, lattice resonances, periodic arrays, nanoparticle arrays, plasmonic crystals, light beam

#### INTRODUCTION

Metallic nanostructures are remarkable tools to manipulate light at the nanoscale due to their ability to support localized surface plasmons. These excitations, which consist in oscillations of the conduction electrons of the nanostructures, couple strongly to light and produce very large enhancements of the electromagnetic field in their vicinity.<sup>2</sup> As a result, metallic nanoparticles supporting localized plasmons display very large absorption cross sections,<sup>3</sup> which make them behave as very efficient nanoscale light-to-heat transducers. 4-6 Initially regarded as an unwanted side effect, the heat generated by this plasmon-enhanced absorption has recently motivated the development of the field of thermoplasmonics, which seeks to exploit this heat for useful purposes.<sup>8,9</sup> The wide range of applications of thermoplasmonics includes improved photocatalysis, <sup>10,11</sup> cancer therapy, <sup>12,13</sup> drug and gene delivery, <sup>14</sup> thermophotovoltaics, 15 nanoscale welding, 16 epoxy photocuring, <sup>17</sup> and water desalination, <sup>18</sup> to cite a few.

When multiple metallic nanoparticles are placed in the vicinity of one another, the localized plasmons that each of them support interact, thus modifying the overall optical properties of the system. <sup>19</sup> Of particular interest is the case in which identical nanoparticles are arranged in a periodic array. Under the right conditions, these systems are able to support

collective modes known as lattice resonances<sup>20–22</sup> that are the result of the coherent multiple scattering between the elements of the array enabled by the periodicity of the system.<sup>23,24</sup> Due to their collective nature, lattice resonances, which appear in the spectrum at wavelengths commensurate with the periodicity of the array, produce strong<sup>25-27</sup> and spectrally narrow optical responses, 28-32 thus making these systems an ideal platform for developing novel biosensors, 33-36 lightemitting devices, 37-42 and color filters, 43-45 among other applications.

Periodic arrays of metallic nanoparticles have been investigated in the context of thermoplasmonics, 46 finding that, under certain illumination conditions, there exists a collective heating effect in which the temperature reached by the nanoparticles in the array can be significantly different than the one they would achieve if they were isolated. 46-48 This effect is the result of each nanoparticle acting as a heat source

Received: October 13, 2022 Published: December 27, 2022





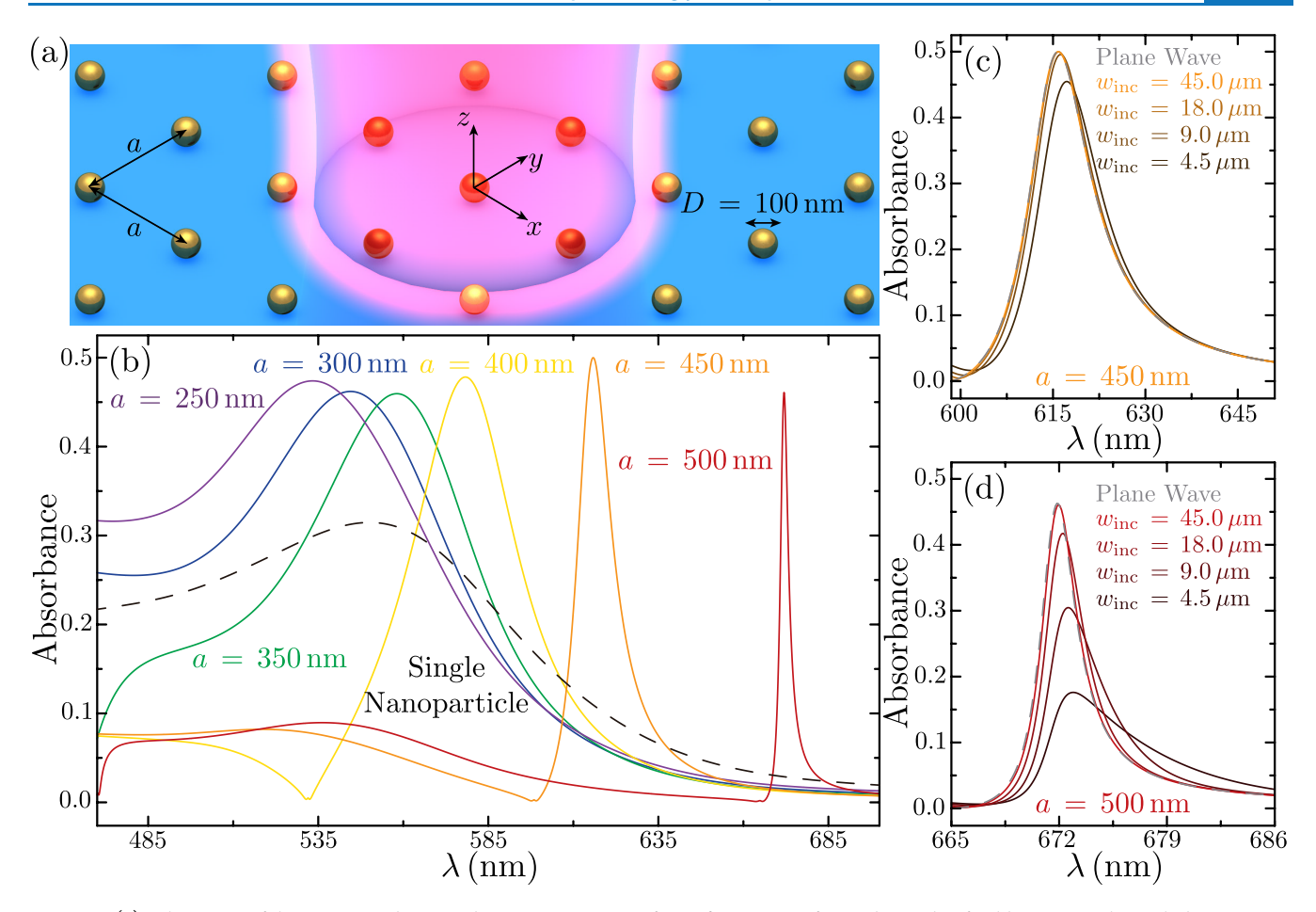


**Figure 1.** (a) Schematics of the system under consideration, consisting of an infinite array of period a made of gold nanoparticles with diameter D=100 nm. The array is surrounded by water and excited by a predominantly x-polarized light beam of finite width with a Gaussian profile, which propagates along the negative z-axis and is centered at the origin (i.e., x=y=0). (b) Absorbance spectra for arrays with different periods a, as indicated by the labels, and for a single nanoparticle (black dashed curve). In all cases,  $w_{\rm inc}=45.0~\mu{\rm m}$ . (c, d) Zoom-in of the spectral region around the lattice resonance for the arrays with  $a=450~{\rm nm}$  (c) and  $a=500~{\rm nm}$  (d). In this case, the different color curves correspond to the results for different values of  $w_{\rm inc}$  as indicated by the legend, while the gray dashed curves show the response to plane-wave illumination.

for the rest of the elements of the array and occurs even when the nanoparticles are considered optically independent, that is, when the optical interactions between them are negligible. While this has been the case for most of the systems considered in the past, recent work has studied the effect of the optical interactions between the nanoparticles in different types of arrangements. However, none of the systems studied in the past fulfill the conditions to support lattice resonances.

Here, we investigate a completely different scenario, in which the periodicity of the array is such that the system supports a collective lattice resonance. Using a rigorous coupled dipole model, we show that the excitation of a lattice resonance produces a significant enhancement of the power absorbed per nanoparticle, which, under pulsed illumination conditions, results in a much larger temperature increase than for arrays that do not support such a mode. In contrast, under continuous wave illumination, the temperature increase of the nanoparticles is largely independent of the period of the array. Furthermore, because the wavelength of the lattice resonance is controlled by the period of the array, it is possible to tune the absorption peak of the system even to wavelengths for which the material and geometrical properties of the individual nanoparticles prevent them from efficiently absorbing light. We

also demonstrate how periodic arrays with two nanoparticles per unit cell can be engineered to support two different lattice resonances, each of them sustained by one of the nanoparticles, thus allowing them to selectively absorb the incident light. Our results show that the lattice resonances supported by periodic arrays of metallic nanoparticles constitute a powerful tool for developing applications in the field of thermoplasmonics, thanks to both their enhanced absorption per nanoparticle and their spectral tunability.

#### ■ RESULTS AND DISCUSSION

We consider an infinite square array of period a composed of spherical nanoparticles with diameter D, as depicted in Figure 1a. The nanoparticles are made of gold, whose dielectric function we take from the tabulated data of ref 53, and they are located in water, with a uniform refractive index of n=1.33. We assume the size of the nanoparticles to be considerably smaller than both the array period a and the relevant wavelengths of light in the dielectric environment  $\lambda/n$  (notice that we use  $\lambda$  to denote the wavelength of light in vacuum). This allows us to model them as point dipoles with polarizability  $\alpha$ , which we calculate from the dipolar Mie scattering coefficient. S4 Within this limit, the response of the whole array can be described using the coupled dipole

model,<sup>23,24,55–59</sup> which, as shown in Figure S1 of the Supporting Information, is in excellent agreement with rigorous solutions of Maxwell's equations obtained using a multiple elastic scattering of multipole expansions (MESME) approach.<sup>54,60</sup>

We calculate the absorbance of the array from the ratio between the power that it absorbs from the incident light beam P and the total power that is incident on it  $P_{\text{inc}}$ . Under the coupled dipole model, the former is given by (see the Methods section)

$$P = \frac{cka^2}{2\pi^2} \int_{1BZ} d\mathbf{k}_{\parallel} \left( \frac{\operatorname{Im}\{\alpha\}}{|\alpha|^2} - \frac{2}{3}nk^3 \right) |\mathbf{p}(\mathbf{k}_{\parallel})|^2$$
 (1)

where the integral is performed over the first Brillouin zone of the array. In this expression, c is the speed of light in vacuum,  $k=2\pi/\lambda$  is the corresponding wavenumber, and  $\mathbf{p}(\mathbf{k}_{\parallel})=\mathcal{A}(\mathbf{k}_{\parallel})\tilde{\mathbf{E}}(\mathbf{k}_{\parallel})$ , with  $\mathcal{A}(\mathbf{k}_{\parallel})=[\alpha^{-1}I_{3\times3}-\mathcal{G}(\mathbf{k}_{\parallel})]^{-1}$  being the polarizability of the array and  $\mathcal{G}(\mathbf{k}_{\parallel})$  being the lattice sum. <sup>23,61</sup> Furthermore,  $\tilde{\mathbf{E}}(\mathbf{k}_{\parallel})$  represents the  $\mathbf{k}_{\parallel}$  components of the electric field of the incident light beam, whose expression is given in the Methods section. Specifically, we consider the array to be excited by a light beam with a finite width that is primarily polarized along the x-axis and propagates along the negative z-axis. The beam is centered at the origin (i.e., x=y=0) and has a Gaussian profile whose width is controlled by the parameter  $w_{\rm inc}$ .

Figure 1b displays the absorbance of arrays with different periods under excitation by such a light beam with  $w_{inc} = 45.0$  $\mu$ m. As indicated by the labels, the colored curves represent the results for different values of a, ranging from 250 to 500 nm. In all cases, the peak absorbance reaches values of nearly 0.5, the maximum absorbance that a two-dimensional array of electric dipoles can achieve under plane-wave illumination. 62 However, the wavelength at which the peak absorbance occurs spans from  $\sim$ 533 nm for a = 250 nm to  $\sim$ 672 nm for a = 500 nm. Furthermore, the resonances for the arrays with smaller values of a have much broader lineshapes, which become significantly narrower as a increases. This can be attributed to the fact that the resonances supported by the arrays with smaller period are not truly collective lattice resonances, as the ones supported by arrays with larger a, but rather are dominated by the localized plasmon of the individual nanoparticles.<sup>63</sup> We can understand this from the fact that lattice resonances appear at the poles of the array polarizability  $\mathcal{A}(\mathbf{k}_{\parallel})$ , which, for excitation with an xpolarized field, are approximately located at the wavelengths for which Re{ $\alpha^{-1}$ } and Re{ $\mathcal{G}_{xx}(\mathbf{k}_{\parallel})$ } cancel each other. Such a cancellation occurs on the red side of the so-called Rayleigh anomalies, at which the real part of the lattice sum diverges to  $+\infty$ . For excitation at normal incidence, the first of the Rayleigh anomalies happens at  $\lambda = na$ . As the period of the array increases, the Rayleigh anomaly moves beyond the wavelength of the localized plasmon resonance of the nanoparticle. As a consequence, Re $\{\alpha^{-1}\}$  takes increasingly large positive values, thus forcing the cancellation condition to shift closer to the Rayleigh anomaly, where  $Re\{\mathcal{G}_{rr}(\mathbf{k}_{\parallel})\}$  is also increasingly large. Since the lattice sum represents the strength of the interactions between the nanoparticles of the array, a larger value corresponds to a lattice resonance for which these interactions play a bigger role and, therefore, is more collective in nature.<sup>64</sup>

Importantly, as a lattice resonance becomes more collective, it demands that a larger number of nanoparticles be uniformly excited in order to sustain it. This means that, if the light beam that is used to excite the array is not wide enough to uniformly illuminate a sufficiently large number of nanoparticles, the lattice resonance will not be efficiently excited, thus resulting in a weaker absorbance than could otherwise be obtained.<sup>64</sup> On the other hand, once the light beam is wide enough to fully excite the lattice resonance, the response of the array does not improve by further increasing  $w_{\rm inc}$ . At this point, the system reaches the limiting case of plane-wave excitation, as we have shown recently.<sup>64</sup> For this reason, we can understand the collectiveness of a lattice resonance from the way that the optical response of the array evolves with  $w_{inc}$ . We perform this analysis for a = 450 nm and a = 500 nm in Figure 1c and d, respectively. As indicated by the legends, we consider  $w_{\rm inc}$ ranging from 4.5 to 45.0  $\mu$ m, with lighter curves corresponding to larger values of  $w_{inc}$ . For comparison, we show the response of the array to plane-wave excitation using a dashed gray curve. Examining these results, we observe that, for a = 500 nm, whose lattice resonance is the most collective out of the arrays we consider, only the light beam with  $w_{\rm inc} = 45.0 \ \mu \rm m$  produces a response that is fully converged to the plane-wave excitation limit. On the other hand, for a = 450 nm, the results for  $w_{inc} =$ 9.0  $\mu$ m are already practically indistinguishable from those for a plane wave, since, in this case, the lattice resonance is not as collective.

The rest of the arrays that we study (i.e., a = 400 nm, a =350 nm, a = 300 nm, and a = 250 nm) support resonances that are less collective in nature. As shown in Figure S2 of the Supporting Information, even for the smallest  $w_{inc}$  that we consider, the absorbance for these systems is identical to their corresponding plane-wave excitation limit. However, the array with a = 400 nm is still much more collective than the ones with a < 400 nm. This can be seen from the fact that the resonance for a = 400 nm is narrower than those of the arrays with smaller a. Moreover, this resonance, which occurs at a wavelength of ~578 nm, is close to the Rayleigh anomaly of the array. For a = 400 nm, this feature appears at 532 nm and is characterized by a sharp dip in the absorbance. In contrast, the absorbance spectra of the arrays with a = 350 nm, a = 300nm, and a = 250 nm are broader and appear much farther from their corresponding Rayleigh anomalies, which all occur at wavelengths outside of the spectral range under consideration. Indeed, the responses of these arrays resemble the localized plasmon of the individual nanoparticles, which we show with a black dashed curve in Figure 1b. Specifically, we plot the absorption cross-section of a single gold nanoparticle, normalized to the unit cell area for the array with a = 250nm. Clearly, the resonances for the arrays with a < 400 nm have a similar shape to that of the single nanoparticle, although they show differences in the peak value, spectral position, and width. Incidentally, this comparison between the response of the single nanoparticle and the different arrays highlights the importance of taking into account interactions between the nanoparticles, since they can lead to relevant differences both when the response is very collective, as well as when it is not, but for different reasons. In the latter case, the differences arise primarily from near-field interactions with the nearest neighbors. In the former case, however, the response is dominated by lattice resonances, which originate from the farfield interaction between the nanoparticles and therefore would not exist without it.

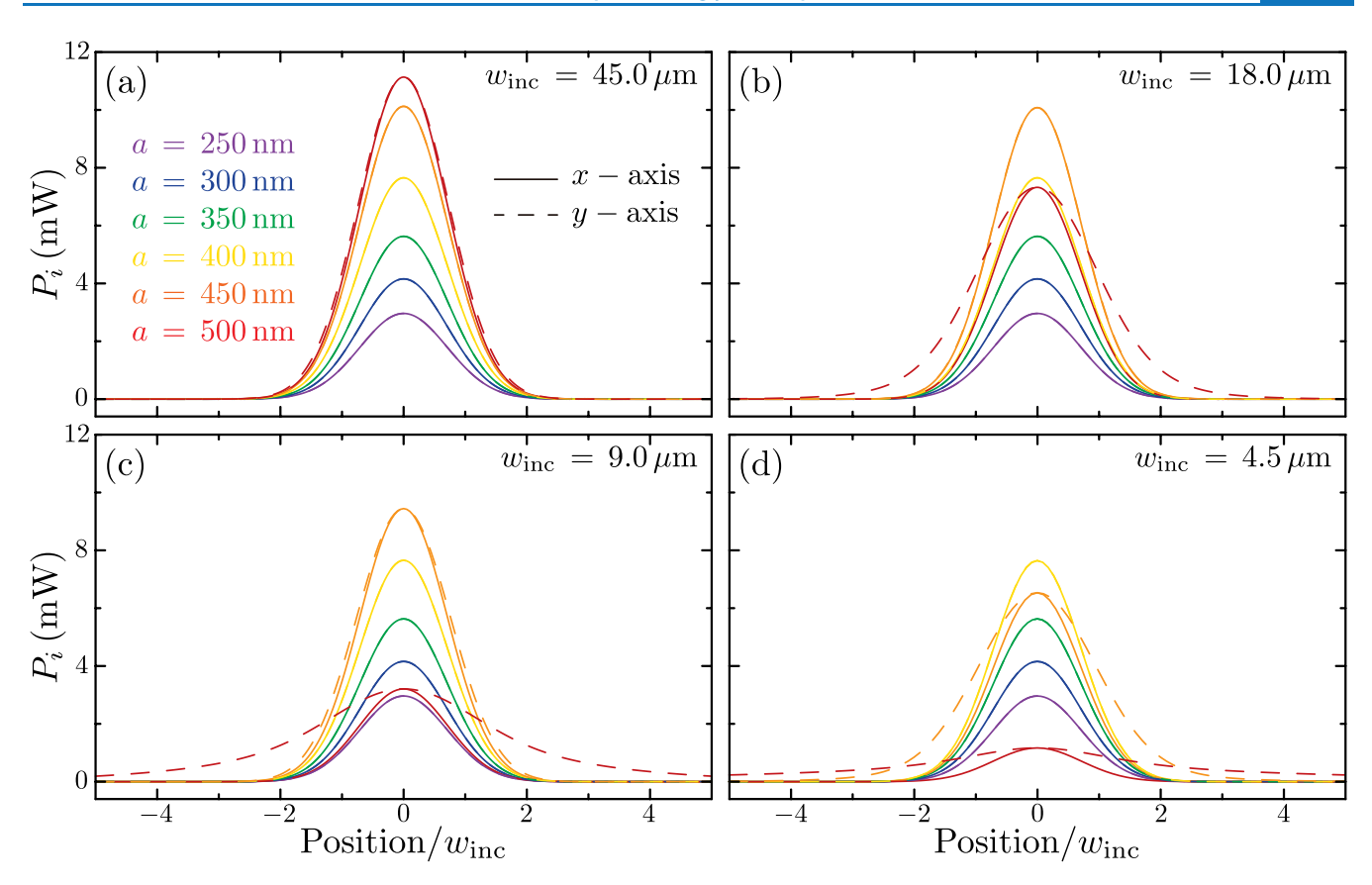


**Figure 2.** Power absorbed by the nanoparticles located along the *x*-axis (solid curves) and *y*-axis (dashed curves) for the arrays of Figure 1b, when illuminated by a finite-width light beam with  $w_{\rm inc} = 45.0~\mu{\rm m}$  (a),  $w_{\rm inc} = 18.0~\mu{\rm m}$  (b),  $w_{\rm inc} = 9.0~\mu{\rm m}$  (c), and  $w_{\rm inc} = 4.5~\mu{\rm m}$  (d). In all cases, we consider the wavelength at which the absorbance of the array is maximum and assume an average intensity of  $\langle I_{\rm inc} \rangle = 10^{11}~{\rm W~m}^{-2}$  for the incident light beam.

Figures 1b and S2 show that, once  $w_{\rm inc}$  is sufficiently large for the response of the array to be converged to the plane-wave excitation limit, all of the arrays under consideration reach a peak absorbance of nearly 0.5. However, it is important to note that, due to their different periods, the arrays have a different number of nanoparticles per unit of area, which is proportional to  $1/a^2$ . As a consequence, for the same absorbance, the power absorbed by each of the individual nanoparticles in the arrays has to scale as  $a^2$ . For instance, considering the arrays with a = 250 nm and a = 500 nm, the individual nanoparticles in the latter case must absorb 4 times as much for both arrays to exhibit the same absorbance.

In order to confirm this hypothesis, we analyze, in Figure 2, the power absorbed by the individual nanoparticles  $P_i$ , for all of the arrays of Figure 1b. We focus on the nanoparticles located along both the *x*-axis (solid curves) and *y*-axis (dashed curves), and perform the calculation of  $P_i$  using eq 5 in the Methods section, for the wavelengths at which each array reaches its maximum absorbance. Each panel corresponds to a different value of  $w_{\rm inc}$ : 45.0 (a), 18.0 (b), 9.0 (c), and 4.5  $\mu$ m (d). Furthermore, to allow for direct comparison between the results for different  $w_{\rm inc}$ , we choose  $P_{\rm inc}$  such that the incident light beam has the same average intensity  $\langle I_{\rm inc} \rangle = P_{\rm inc}/(\pi w_{\rm inc}^2) = 10^{11}$  W m<sup>-2</sup> in all cases.

As anticipated, for  $w_{\rm inc} = 45.0~\mu{\rm m}$  (Figure 2a), the power absorbed by the individual nanoparticles is smallest for the array with  $a = 250~{\rm nm}$  and maximum for  $a = 500~{\rm nm}$ , with the latter being almost four times larger than the former. Moreover, the slices along the x- and y-axes are identical to

one another, except for a = 500 nm, though, in that case, they are still nearly indistinguishable. The situation is different, however, when the light beam is not wide enough to efficiently excite the lattice resonance, as is the case for the array with a =500 nm when  $w_{\rm inc} = 18.0 \ \mu \text{m}$  (Figure 2b). In this situation, a significant asymmetry appears, with the slice along the y-axis becoming remarkably wider than the one along the x-axis. The explanation for this behavior is that, as we have recently shown in ref 64, when  $w_{\rm inc}$  is not large enough for the response of the array to be converged to the plane-wave excitation limit, the spatial extension of the lattice resonance exceeds that of the incident light beam. However, this only happens along the direction of propagation of the lattice resonance, which is always perpendicular to the polarization of the light beam that excites it. In addition, the power absorbed by the individual nanoparticles of the array is significantly reduced, becoming lower than the results for a = 400 nm. For the rest of the arrays, on the other hand, the light beam is still able to efficiently excite their resonances and, thus, the power absorbed by the individual nanoparticles remains completely unchanged. A further reduction in  $w_{inc}$  to 9.0  $\mu$ m (Figure 2c) and 4.5  $\mu$ m (Figure 2d) allows the trend to continue. In particular, for  $w_{\rm inc}$  = 9.0  $\mu$ m, the power absorbed by the nanoparticles in the array with a = 500 nm drops below that of every array under consideration except for the one with a =250 nm. Meanwhile, the array with a = 450 nm still shows the largest power absorbed by the nanoparticles, although a slight asymmetry begins to appear. However, for  $w_{\rm inc} = 4.5 \ \mu \rm m$ , the power absorbed by the nanoparticles in the a = 450 nm array

drops as well, since the lattice resonance is not fully excited. This leaves the array with a=400 nm as the optimum, with the lowest power absorbed corresponding to the array with a=500 nm.

Another way of visualizing the trends of Figure 2 is by considering only  $P_0$ , the power absorbed by the central nanoparticle (i.e., the one located at the origin). Since the origin is also where the light beam is centered, this nanoparticle is the one that absorbs the most power. We plot  $P_0$  as a function of a in Figure 3, using the left scale, for the

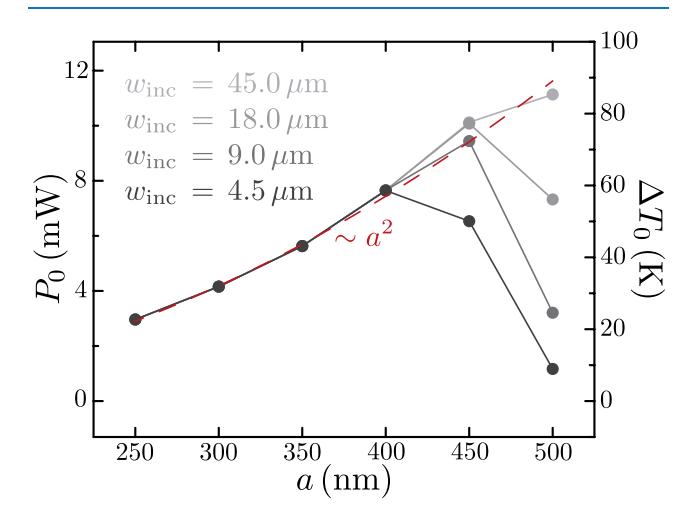


**Figure 3.** The left scale shows the power absorbed by the central nanoparticle of the arrays,  $P_0$ , as a function of a for the different  $w_{\rm inc}$  indicated by the legend. We perform the calculations at the wavelength at which the absorbance of the array is maximum and assume an average intensity of  $\langle I_{\rm inc} \rangle = 10^{11} \ {\rm W m^{-2}}$  for the incident light beam. The right scale shows the temperature increase of the central nanoparticle of the array under pulsed illumination conditions. The red dashed curve indicates a quadratic scaling with a.

same values of  $w_{\text{inc}}$  considered before. As indicated by the legend, the lightest curve displays the results for  $w_{\rm inc} = 45.0$  $\mu$ m, with darker ones corresponding to smaller  $w_{\rm inc}$ . For values of a up to 400 nm, P<sub>0</sub> almost perfectly follows a quadratic dependence on a, as can be seen by comparing it with the red dashed curve. Furthermore, in this range, all of the curves lie directly on top of one another, since, as we discussed before, the smallest  $w_{inc}$  already saturates the response of these arrays to the plane-wave limit. The situation starts to differ when a is increased to 450 nm. In this case, while, for the largest values of  $w_{\rm inc}$ ,  $P_0$  still approximately follows the  $a^2$  dependence, its value drops significantly for  $w_{\rm inc}$  = 4.5  $\mu$ m. As expected, this effect is more pronounced for a = 500 nm, for which only the value of  $P_0$  for  $w_{\rm inc} = 45.0 \ \mu \rm m$  remains close to the quadratic trend. These results confirm that, as long as the light beam is wide enough to efficiently excite the lattice resonance, the power absorbed by the central nanoparticle grows approximately as  $a^2$ .

Importantly, the power absorbed by the central nanoparticle can be used to estimate the increase in temperature that it would undergo under pulsed illumination. Specifically, following ref 65 and assuming that the duration of the pulse  $\tau$  is shorter than the time it takes for the nanoparticles to thermalize with their environment, we can write the temperature increase of the central nanoparticle for a single pulse as

$$\Delta T_0 = \frac{\epsilon_0}{V \rho_{\text{Au}} c_{\text{Au}}} \tag{2}$$

where  $V = \pi D^3/6$  is the volume of the nanoparticle,  $\rho_{\rm Au}$  = 19320 kg m<sup>-3</sup> is the mass density of gold and  $c_{Au} = 129 \text{ J kg}^{-1}$  $K^{-1}$  its specific heat capacity. Furthermore,  $\epsilon_0$  is the energy absorbed by the nanoparticle. Here, we choose  $\tau = 10$  ps, which is short enough for eq 2 to be valid but sufficiently long for the light beam to be considered quasimonochromatic. This allows us to approximate the energy absorbed by the nanoparticle as  $\epsilon_0 \approx P_0 \tau$ . The results of this calculation are displayed with the right scale of Figure 3, for the different arrays and incident light beams under consideration. Since, following eq 2,  $\Delta T_0$  depends linearly on  $P_0$ , the same trends discussed before for this quantity hold true. Notably, this means that the temperature increase grows quadratically with the period of the array. This is true as long as the incident light beam is sufficiently wide to fully excite their lattice resonance. For instance, the temperature increase for a = 500 nm and  $w_{inc}$ = 45  $\mu$ m is nearly four times what is achieved with the same average intensity incident on the array with a = 250 nm.

The situation is different, however, when the array is subject to continuous wave illumination conditions. In this case, there is a collective heating effect between the nanoparticles,  $^{46,47}$  in which each one acts as a heat source for the rest. As a consequence, the temperature increase for the central nanoparticle of an array can be computed as the sum of two terms  $^{46,47}$ 

$$\Delta T_0^{\text{CW}} = \frac{P_0}{2\pi\kappa D} + \sum_{i\neq 0} \frac{P_i}{4\pi\kappa |\mathbf{R}_i|}$$
(3)

where  $\kappa = 0.6~\mathrm{W~m^{-1}~K^{-1}}$  is the thermal conductivity of water and the sum runs over all of the nanoparticles in the array except for the central one. The first term in the expression corresponds to the temperature increase due to the direct absorption of the central nanoparticle, while the second term represents the collective heating effect produced by the rest of the nanoparticles in the array. Notably, this portion of the expression decays with the distance  $|\mathbf{R}_i|$  of the nanoparticles from the origin. Therefore, when analyzing the temperature increase of the central nanoparticle, we anticipate an interplay between the enhanced absorption per nanoparticle for the arrays supporting collective lattice resonances and the diminished contributions of collective heating due to the larger separation between the nanoparticles.

Figure 4 shows  $\Delta T_0^{\text{CW}}$  as a function of a for the different values of  $w_{inc}$  indicated by the legend. We perform the calculations at the wavelengths at which the arrays reach their maximum absorbance and assume a constant average intensity  $\langle I_{\rm inc} \rangle$  = 5 × 10<sup>6</sup> W m<sup>-2</sup>, which yields temperature increases on the order of tens of Kelvins. Examining these results, we observe that, for a given  $w_{\text{inc}}$ ,  $\Delta T_0^{\text{CW}}$  does not vary significantly with a, as long as the incident light beam is sufficiently wide to efficiently excite the resonance supported by the arrays. We attribute this behavior to the aforementioned interplay between the increased absorption per nanoparticle and the diminished collective heating effect as a grows. In particular, when  $w_{\rm inc}$  is sufficiently large, the second term of eq 3 dominates  $\Delta T_0^{\text{CW}}$ . Furthermore, as shown in Figure 2, the power absorbed per nanoparticle increases as  $a^2$  and follows a Gaussian spatial distribution, that is,  $P_i \propto a^2 e^{-|\mathbf{R}_i|^2/w_{\text{inc}}^2}$ . Then, performing the transformation  $|\mathbf{R}_i| \to \rho a$  and approximating

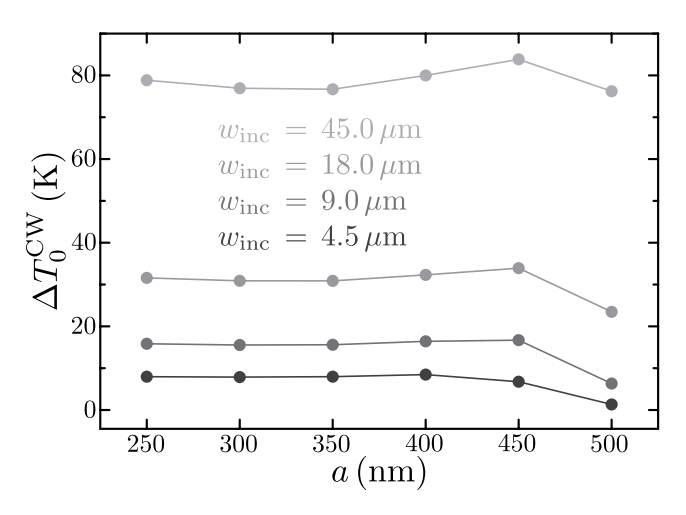


**Figure 4.** Temperature increase for the central nanoparticle of the different arrays under consideration for continuous wave illumination conditions. As indicated by the legend, the different curves represent different values of  $w_{\rm inc}$ . In all cases, we perform the calculations at the wavelength of maximum absorption and assume  $\langle I_{\rm inc} \rangle = 5 \times 10^6 \ {\rm W}$  m<sup>-2</sup> for the average intensity of the incident light beam.

the sum in eq 3 as an integral over  $\rho$ , one can demonstrate that  $\Delta T_0^{\rm CW}$  is approximately independent of the array period. It is also important to note that, in contrast to the results for pulsed illumination conditions, the temperature increase achieved by the central nanoparticle does depend on the value of  $w_{\rm inc}$ . Indeed, increasing  $w_{\rm inc}$  from 4.5 to 45.0  $\mu$ m yields approximately an order of magnitude growth in  $\Delta T_0^{\rm CW}$ . Such a result is completely expected since, in the latter case, the light beam is uniformly exciting an area that is approximately a hundred times larger, producing a significantly stronger collective heating effect.

So far, we have focused on arrays of nanoparticles that are formed from the repetition of a unit cell containing a single element. However, there has recently been significant interest in the lattice resonances supported by arrays with multiparticle unit cells<sup>23,32,66–70</sup> and, in particular, bipartite arrays.<sup>59,71</sup> Such systems enable a greater degree of control over the optical response of the array, since, depending on the relative positions of the nanoparticles within the unit cell, the lattice resonances supported by the array can have very different properties.<sup>23,59</sup> In the context of thermoplasmonics, this can be exploited to engineer complex heating scenarios, such as the selective heating of a subset of nanoparticles.

To illustrate this possibility, we consider the bipartite array depicted in the inset schematics of Figure 5. The array has a period a = 450 nm and its unit cell is composed of two gold nanoparticles with diameters 80 and 120 nm. The smaller nanoparticle is located at the origin of the unit cell, while the larger one is placed at a distance a/2 along the x-axis and a/4along the y-axis from the other one. The black curve in Figure 5 shows the absorbance spectrum for this array when excited by a light beam with  $w_{\rm inc} = 45.0 \ \mu \rm m$ . We perform this calculation by extending eq 1 to bipartite arrays following the approach described in refs 23 and 59. The particular arrangement of the nanoparticles in the unit cell makes this system support two different lattice resonances, each of which is sustained by one of the nanoparticles.<sup>23</sup> This can be seen by analyzing the contributions of each nanoparticle to the total absorbance of the array, which are displayed by the orange and

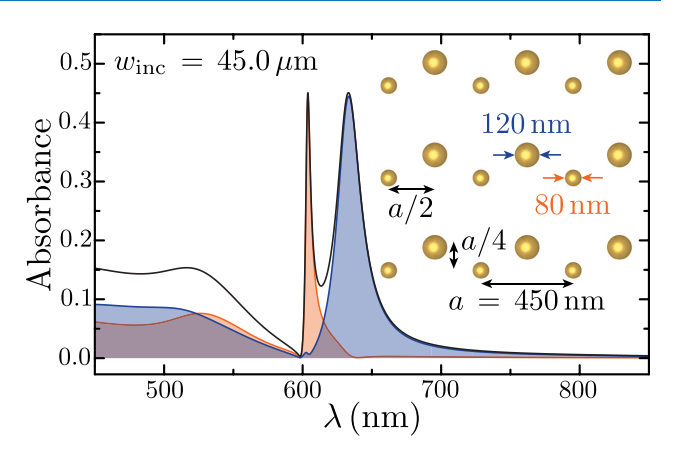


**Figure 5.** Absorbance for a bipartite array. As depicted in the inset schematics, the array is built from the repetition of a unit cell containing two gold nanoparticles over a square lattice of period a=450 nm. The smaller nanoparticle has a diameter of 80 nm and is located at the origin of the unit cell, while the larger one has a diameter of 120 nm and is displaced with respect to the other nanoparticle by a distance a/2 along the x-axis and a/4 along the y-axis. The orange and blue shaded areas show, respectively, the contributions of the smaller and larger nanoparticles to the absorbance of the array when excited by a light beam with  $w_{\rm inc}=45.0~\mu{\rm m}$ , while the black curve shows the total absorbance of the array under the same excitation conditions.

blue shaded areas, respectively, for the smaller and larger nanoparticles. The absorbance of the smaller nanoparticle reaches a peak value of ~0.45 at a wavelength ~604 nm, while, for the larger one, a similar peak value is achieved at  $\lambda \sim 633$  nm. Importantly, the absorbance of each of the nanoparticles is practically negligible at the wavelength at which the other one reaches its maximum. Therefore, by using the appropriate wavelength, the absorption of the array can be directed toward one of the nanoparticles in the unit cell without exciting the other one. These results demonstrate that it is possible to selectively heat nanoparticles within an appropriately designed multipartite array, thus highlighting the potential of the lattice resonances of periodic arrays for achieving a high degree of control in thermoplasmonics applications.

#### CONCLUSIONS

In summary, we have explored the use of the lattice resonances of periodic arrays of nanoparticles for thermoplasmonics. Using a rigorous coupled dipole model, we have shown that arrays supporting collective lattice resonances absorb more power per nanoparticle than those that do not support such modes. In particular, the power absorbed per nanoparticle scales with the inverse of the density of nanoparticles in the array, as long as the incident light beam is sufficiently wide to efficiently excite the lattice resonance. This means that, under pulsed illumination, for which there is no collective heating effect, the temperature increase of the nanoparticles in the array grows with the square of its period. In contrast, under continuous wave illumination conditions, we have found that the temperature increase is almost independent of the period of the array. We have shown that this behavior originates from the interplay between the enhancement of the power absorbed per nanoparticle provided by the lattice resonances, which increases with the period, and the collective heating effect, which behaves conversely. We have also investigated the response of bipartite arrays and demonstrated that, when

appropriately engineered, these systems support two independent lattice resonances, each of them sustained by one of the nanoparticles. These modes can be exploited to selectively absorb the incident light in one of the nanoparticles without exciting the other. Furthermore, since the spectral position of the lattice resonance is determined by the period of the array, it is possible to tune the absorption peak of the array to wavelengths at which the nanoparticles would not absorb individually. The enhanced absorption per nanoparticle, together with the control and tunability provided by lattice resonances, makes them a useful tool for applications in thermoplasmonics. In particular, we anticipate that our results are of great value for applications that depend nonlinearly on the temperature increase. For instance, chemical reactions that involve overcoming a potential barrier would benefit exponentially from the greater temperature increase achieved under pulsed illumination conditions for periodic arrays of nanoparticles supporting lattice resonances. The results of our work provide a strong theoretical understanding of the benefits that lattice resonances can bring to thermoplasmonics.

#### METHODS

**Optical Response of the Array.** To describe the response of an infinite array, we use the coupled dipole model.<sup>23,24</sup>, Within this approach, the dipole induced in the nanoparticle located at position  $\mathbf{R}_i$  can be written as  $\mathbf{p}_i = \alpha \mathbf{E}_i + \alpha \sum_{i \neq i} \mathbf{G}_{ii} \mathbf{p}_{i'}$ where  $\mathbf{E}_i$  is the incident field at the position of the nanoparticle. Moreover,  $\mathbf{G}_{ij} = [(nk)^2 I_{3\times 3} + \nabla \hat{\nabla}] e^{ink|\mathbf{R}_i - \mathbf{R}_j|} / (n^2 |\mathbf{R}_i - \mathbf{R}_j|)$  is the dipole-dipole interaction tensor between nanoparticles located at  $\mathbf{R}_i$  and  $\mathbf{R}_j$ , with  $\mathcal{I}_{3\times3}$  being the 3 × 3 identity matrix. We can use the Fourier transform, defined as  $\mathbf{p}_{i}=rac{a^{2}}{4\pi^{2}}\int_{\mathrm{1BZ}}d\mathbf{k}_{\parallel}\mathbf{p}(\mathbf{k}_{\parallel})e^{i\mathbf{k}_{\parallel}\mathbf{R}_{i}}$  for the induced dipole and similarly for other quantities, to obtain  $\mathbf{p}(\mathbf{k}_{\parallel}) = \alpha \tilde{\mathbf{E}}(\mathbf{k}_{\parallel}) + \alpha \mathcal{G}(\mathbf{k}_{\parallel}) \mathbf{p}(\mathbf{k}_{\parallel})$ . In this expression,  $\mathcal{G}(\mathbf{k}_{\parallel}) = \sum_{i \neq i} \mathbf{G}_{ij} e^{-i\mathbf{k}_{\parallel}(\mathbf{R}_i - \mathbf{R}_j)}$  is the lattice sum, and  $\tilde{\mathbf{E}}(\mathbf{k}_{\parallel})$  are the  $\mathbf{k}_{\parallel}$  components of the electric field of the incident light beam within the first Brillouin zone, as we discuss below. This self-consistent system of equations can be solved as

$$\mathbf{p}(\mathbf{k}_{\parallel}) = \mathcal{A}(\mathbf{k}_{\parallel})\tilde{\mathbf{E}}(\mathbf{k}_{\parallel})$$

where  $\mathcal{A}(\mathbf{k}_{\parallel}) = [\alpha^{-1}I_{3\times3} - \mathcal{G}(\mathbf{k}_{\parallel})]^{-1}$  is the polarizability of the array. Therefore, the dipole induced in the nanoparticle located at  $\mathbf{R}_i$  is given by

$$\mathbf{p}_{i} = \frac{a^{2}}{4\pi^{2}} \int_{1BZ} d\mathbf{k}_{\parallel} \mathcal{A}(\mathbf{k}_{\parallel}) \tilde{\mathbf{E}}(\mathbf{k}_{\parallel}) e^{i\mathbf{k}_{\parallel} \mathbf{R}_{i}}$$
(4)

which allows us to calculate the power absorbed by the individual nanoparticles as

$$P_{i} = 2kc \left[ \frac{\operatorname{Im}\{\alpha\}}{|\alpha|^{2}} - \frac{2}{3}nk^{3} \right] |\mathbf{p}_{i}|^{2}$$
(5)

Then, the power absorbed by the whole array is given by  $P = \sum_i P_i$ , which, using the expression  $\sum_i e^{i(\mathbf{k}_{\parallel} - \mathbf{k}_{\parallel}') \cdot \mathbf{R}_i} = \frac{4\pi^2}{a^2} \sum_{\mathbf{q}} \delta(\mathbf{k}_{\parallel} - \mathbf{k}_{\parallel}' + \mathbf{q})$ , yields eq 1. Notice that  $\mathbf{q}$  represents the reciprocal lattice vectors of the array, defined as  $\mathbf{q} = 2\pi [l\hat{\mathbf{x}} + m\hat{\mathbf{y}}]/a$ , with l and m being integers.

**Incident Field.** We assume the arrays to be excited by a mainly *x*-polarized beam of finite width and a Gaussian spatial

profile. The electric field of this beam at position  $\mathbf{R}_i$  is given by  $^{64}$ 

$$\mathbf{E}_{i} = \frac{1}{4\pi^{2}} \int_{\|\mathbf{k}_{\parallel} \le nk} d\mathbf{k}_{\parallel} \mathbf{E}(\mathbf{k}_{\parallel}) e^{i\mathbf{k}_{\parallel} \mathbf{R}_{i}}$$

where  $\mathbf{E}(\mathbf{k}_{\parallel}) = E_{\rm inc}[\hat{\mathbf{x}} - \hat{\mathbf{z}}k_x/k_z] \ f(|\mathbf{k}_{\parallel}|), \ f(|\mathbf{k}_{\parallel}|) = 2\pi w_{\rm inc}^2 \exp[-w_{\rm inc}^2|\mathbf{k}_{\parallel}|^2/2], \ E_{\rm inc}$  is a constant, and  $w_{\rm inc}$  is a parameter that controls the width of the beam. Note that, for  $\mathbf{E}_i$  to satisfy Maxwell's equations,  $\mathbf{E}(\mathbf{k}_{\parallel}) \cdot [\mathbf{k}_{\parallel} + k_z \hat{\mathbf{z}}] = 0$ , where  $k_z = \sqrt{n^2 k^2 - |\mathbf{k}_{\parallel}|^2}$ . This condition forces the electric field to have a nonzero longitudinal component, although it is mainly polarized along the x-axis. Moreover, while this integral is restricted to the light cone,  $|\mathbf{k}_{\parallel}| \leq nk$ , the integrals in eqs 1 and 4 run over the first Brillouin zone of the array. Therefore, we need to appropriately transform  $\mathbf{E}(\mathbf{k}_{\parallel})$ . This can be done by exploiting the periodicity of the array as  $\tilde{\mathbf{E}}(\mathbf{k}_{\parallel}) = \sum_{\mathbf{q}} \mathbf{E}(\mathbf{k}_{\parallel} + \mathbf{q})/a^2$ , with the sum running over all of the reciprocal lattice vectors that satisfy  $|\mathbf{k}_{\parallel} + \mathbf{q}| \leq nk$ .

As expected, taking the limit  $nkw_{inc} \gg 1$  in any of the expressions yields the results for a plane wave.

#### ASSOCIATED CONTENT

#### **5** Supporting Information

The Supporting Information is available free of charge at https://pubs.acs.org/doi/10.1021/acsphotonics.2c01610.

Benchmark of the coupled dipole model against rigorous solutions of Maxwell's equations. Absorption spectra for the arrays of Figure 1 excited by a light beam with different values of  $w_{\rm inc}$  (PDF)

#### AUTHOR INFORMATION

#### **Corresponding Author**

Alejandro Manjavacas — Department of Physics and Astronomy, University of New Mexico, Albuquerque, New Mexico 87106, United States; Instituto de Optica (IO-CSIC), Consejo Superior de Investigaciones Científicas, 28006 Madrid, Spain; orcid.org/0000-0002-2379-1242; Email: a.manjavacas@csic.es

#### **Authors**

Lauren Zundel – Department of Physics and Astronomy, University of New Mexico, Albuquerque, New Mexico 87106, United States; orcid.org/0000-0003-1850-5210

Kellen Malone – Department of Physics and Astronomy, University of New Mexico, Albuquerque, New Mexico 87106, United States

Luis Cerdán – Instituto de Óptica (IO-CSIC), Consejo Superior de Investigaciones Científicas, 28006 Madrid, Spain; ocid.org/0000-0002-7174-2453

Rosario Martínez-Herrero – Departamento de Optica, Universidad Complutense de Madrid, 28040 Madrid, Spain

Complete contact information is available at: https://pubs.acs.org/10.1021/acsphotonics.2c01610

#### **Funding**

BBVA Foundation, Leonardo Grant; Spanish MCIN/AEI/10.13039/501100011033, Grant Nos. PID2019-104268GB-C21 and PID2019-109502GA-I00; U.S. National Science Foundation, Grant No. DMR-1941680; Consejo Superior de Investigaciones Científicas, PIE 202150I030; Department of

Energy Computational Science Graduate Fellowship, Grant No. DE-SC0020347

#### **Notes**

The authors declare no competing financial interest.

#### ACKNOWLEDGMENTS

L.Z. and K.M. contributed equally to this work. This work was sponsored by a Leonardo Grant for Researchers in Physics from the BBVA Foundation. The authors also acknowledge support from Grant Nos. PID2019-104268GB-C21 and PID2019-109502GA-100 funded by MCIN/AEI/10.13039/501100011033 as well as the U.S. National Science Foundation (Grant No. DMR-1941680). A.M. acknowledges support from Consejo Superior de Investigaciones Científicas (PIE 2021501030). L.Z. acknowledges support from the Department of Energy Computational Science Graduate Fellowship (Grant No. DE-SC0020347). We also thank the UNM Center for Advanced Research Computing, supported in part by the U.S. National Science Foundation, for providing some of the computational resources used in this work.

#### REFERENCES

- (1) Maier, S. A. Plasmonics: Fundamentals and Applications; Springer: New York, 2007.
- (2) Álvarez-Puebla, R. A.; Liz-Marzán, L. M.; García de Abajo, F. J. Light concentration at the nanometer scale. *J. Phys. Chem. Lett.* **2010**, 1, 2428–2434.
- (3) Myroshnychenko, V.; Rodríguez-Fernández, J.; Pastoriza-Santos, I.; Funston, A. M.; Novo, C.; Mulvaney, P.; Liz-Marzán, L. M.; García de Abajo, F. J. Modelling the optical response of gold nanoparticles. *Chem. Soc. Rev.* **2008**, *37*, 1792–1805.
- (4) Baffou, G.; Quidant, R.; Girard, C. Heat generation in plasmonic nanostructures: Influence of morphology. *Appl. Phys. Lett.* **2009**, *94*, 153109
- (5) Baffou, G.; Quidant, R.; García de Abajo, F. J. Nanoscale control of optical heating in complex plasmonic systems. *ACS Nano* **2010**, *4*, 709–716.
- (6) Jauffred, L.; Samadi, A.; Klingberg, H.; Bendix, P. M.; Oddershede, L. B. Plasmonic heating of nanostructures. *Chem. Rev.* **2019**, *119*, 8087–8130.
- (7) Baffou, G.; Quidant, R. Thermo-plasmonics: Using metallic nanostructures as nano-sources of heat. *Laser Photonics Rev.* **2013**, 7, 171–187.
- (8) Govorov, A. O.; Richardson, H. H. Generating heat with metal nanoparticles. *Nanotoday* **2007**, *2*, 30–38.
- (9) Baffou, G.; Cichos, F.; Quidant, R. Applications and challenges of thermoplasmonics. *Nat. Mater.* **2020**, *19*, 946–958.
- (10) Baffou, G.; Quidant, R. Nanoplasmonics for chemistry. Chem. Soc. Rev. 2014, 43, 3898–3907.
- (11) Cortés, E.; Besteiro, L. V.; Alabastri, A.; Baldi, A.; Tagliabue, G.; Demetriadou, A.; Narang, P. Challenges in plasmonic catalysis. *ACS Nano* **2020**, *14*, 16202–16219.
- (12) Rastinehad, A. R.; et al. Gold nanoshell-localized photothermal ablation of prostate tumors in a clinical pilot device study. *Proc. Natl. Acad. Sci. U. S. A.* **2019**, *116*, 18590–18596.
- (13) Chen, J.; Gong, M.; Fan, Y.; Feng, J.; Han, L.; Xin, H. L.; Cao, M.; Zhang, Q.; Zhang, D.; Lei, D.; Yin, Y. Collective plasmon coupling in gold nanoparticle clusters for highly efficient photothermal therapy. *ACS Nano* **2022**, *16*, 910–920.
- (14) Han, G.; Ghosh, P.; De, M.; Rotello, V. M. Drug and gene delivery using gold nanoparticles. *NanoBiotechnology* **2007**, *3*, 40–45.
- (15) Zhou, Z.; Sakr, E.; Sun, Y.; Bermel, P. Solar thermophotovoltaics: Reshaping the solar spectrum. *Nanophotonics* **2016**, *5*, 1–21.
- (16) Wang, L.; Feng, Y.; Li, Z.; Liu, G. Nanoscale thermoplasmonic welding. iScience 2022, 25, 104422.

- (17) Roberts, A. T.; Yang, J.; Reish, M. E.; Alabastri, A.; Halas, N. J.; Nordlander, P.; Everitt, H. O. Plasmonic nanoparticle-based epoxy photocuring: A deeper look. *Mater. Today* **2019**, *27*, 14–20.
- (18) Zhou, L.; Tan, Y.; Wang, J.; Xu, W.; Yuan, Y.; Cai, W.; Zhu, S.; Zhu, J. 3D self-assembly of aluminium nanoparticles for plasmonenhanced solar desalination. *Nat. Photonics* **2016**, *10*, 393–398.
- (19) Halas, N. J.; Lal, S.; Chang, W.; Link, S.; Nordlander, P. Plasmons in strongly coupled metallic nanostructures. *Chem. Rev.* **2011**, *111*, 3913–3961.
- (20) Kravets, V. G.; Kabashin, A. V.; Barnes, W. L.; Grigorenko, A. N. Plasmonic surface lattice resonances: A review of properties and applications. *Chem. Rev.* **2018**, *118*, 5912–5951.
- (21) Wang, W.; Ramezani, M.; Väkeväinen, A. I.; Törmä, P.; Gómez Rivas, J.; Odom, T. W. The rich photonic world of plasmonic nanoparticle arrays. *Mater. Today* **2018**, *21*, 303–314.
- (22) Utyushev, A. D.; Zakomirnyi, V. I.; Rasskazov, I. L. Collective lattice resonances: Plasmonics and beyond. *Rev. Phys.* **2021**, *6*, 100051.
- (23) Baur, S.; Sanders, S.; Manjavacas, A. Hybridization of lattice resonances. ACS Nano 2018, 12, 1618–1629.
- (24) Cherqui, C.; Bourgeois, M. R.; Wang, D.; Schatz, G. C. Plasmonic surface lattice resonances: Theory and computation. *Acc. Chem. Res.* **2019**, *52*, 2548–2558.
- (25) Zou, S.; Schatz, G. C. Silver nanoparticle array structures that produce giant enhancements in electromagnetic fields. *Chem. Phys. Lett.* **2005**, 403, 62–67.
- (26) Nikitin, A. G.; Kabashin, A. V.; Dallaporta, H. Plasmonic resonances in diffractive arrays of gold nanoantennas: Near and far field effects. *Opt. Express* **2012**, *20*, 27941–27952.
- (27) Manjavacas, A.; Zundel, L.; Sanders, S. Analysis of the limits of the near-field produced by nanoparticle arrays. *ACS Nano* **2019**, *13*, 10682–10693.
- (28) Le-Van, Q.; Zoethout, E.; Geluk, E.-J.; Ramezani, M.; Berghuis, M.; Gómez Rivas, J. Enhanced quality factors of surface lattice resonances in plasmonic arrays of nanoparticles. *Adv. Opt. Mater.* **2019**, *7*, 1801451.
- (29) Scarabelli, L.; Vila-Liarte, D.; Mihi, A.; Liz-Marzán, L. M. Templated colloidal self-assembly for lattice plasmon engineering. *Acc. Mater. Res.* **2021**, *2*, 816–827.
- (30) Deng, S.; Li, R.; Park, J.-E.; Guan, J.; Choo, P.; Hu, J.; Smeets, P. J. M.; Odom, T. W. Ultranarrow plasmon resonances from annealed nanoparticle lattices. *Proc. Natl. Acad. Sci. U. S. A.* **2020**, *117*, 23380–23384.
- (31) Bin-Alam, M. S.; Reshef, O.; Mamchur, Y.; Alam, M. Z.; Carlow, G.; Upham, J.; Sullivan, B. T.; Ménard, J.-M.; Huttunen, M. J.; Boyd, R. W.; Dolgaleva, K. Ultra-high-Q resonances in plasmonic metasurfaces. *Nat. Commun.* **2021**, *12*, 974.
- (32) Zundel, L.; May, A.; Manjavacas, A. Lattice resonances induced by periodic vacancies in arrays of nanoparticles. *ACS Photonics* **2021**, *8*, 360–368.
- (33) Adato, R.; Yanik, A. A.; Amsden, J. J.; Kaplan, D. L.; Omenetto, F. G.; Hong, M. K.; Erramilli, S.; Altug, H. Ultra-sensitive vibrational spectroscopy of protein monolayers with plasmonic nanoantenna arrays. *Proc. Natl. Acad. Sci. U. S. A.* **2009**, *106*, 19227–19232.
- (34) Thackray, B. D.; Kravets, V. G.; Schedin, F.; Auton, G.; Thomas, P. A.; Grigorenko, A. N. Narrow collective plasmon resonances in nanostructure arrays observed at normal light incidence for simplified sensing in asymmetric air and water environments. *ACS Photonics* **2014**, *1*, 1116–1126.
- (35) Danilov, A.; Tselikov, G.; Wu, F.; Kravets, V. G.; Ozerov, I.; Bedu, F.; Grigorenko, A. N.; Kabashin, A. V. Ultra-narrow surface lattice resonances in plasmonic metamaterial arrays for biosensing applications. *Biosens. Bioelectron.* **2018**, *104*, 102–112.
- (36) Matricardi, C.; Hanske, C.; Garcia-Pomar, J. L.; Langer, J.; Mihi, A.; Liz-Marzán, L. M. Gold nanoparticle plasmonic superlattices as surface-enhanced Raman spectroscopy substrates. *ACS Nano* **2018**, 12, 8531–8539.
- (37) Lozano, G.; Louwers, D. J.; Rodríguez, S. R. K.; Murai, S.; Jansen, O. T. A.; Verschuuren, M. A.; Gómez Rivas, J. Plasmonics for

- solid-state lighting: Enhanced excitation and directional emission of highly efficient light sources. Light Sci. Appl. 2013, 2, e66.
- (38) Zhou, W.; Dridi, M.; Suh, J. Y.; Kim, C. H.; Co, D. T.; Wasielewski, M. R.; Schatz, G. C.; Odom, T. W. Lasing action in strongly coupled plasmonic nanocavity arrays. *Nat. Nanotechnol.* **2013**, *8*, 506–511.
- (39) Schokker, A. H.; Koenderink, A. F. Lasing at the band edges of plasmonic lattices. *Phys. Rev. B* **2014**, *90*, 155452.
- (40) Ramezani, M.; Lozano, G.; Verschuuren, M. A.; Gómez-Rivas, J. Modified emission of extended light emitting layers by selective coupling to collective lattice resonances. *Phys. Rev. B* **2016**, *94*, 125406.
- (41) Guo, R.; Nečada, M.; Hakala, T. K.; Väkeväinen, A. I.; Törmä, P. Lasing at K points of a honeycomb plasmonic lattice. *Phys. Rev. Lett.* **2019**, *122*, 013901.
- (42) Vaskin, A.; Kolkowski, R.; Koenderink, F. A.; Staude, I. Light-emitting metasurfaces. *Nanophotonics* **2019**, *8*, 1151.
- (43) Olson, J.; Manjavacas, A.; Basu, T.; Huang, D.; Schlather, A. E.; Zheng, B.; Halas, N. J.; Nordlander, P.; Link, S. High chromaticity aluminum plasmonic pixels for active liquid crystal displays. *ACS Nano* **2016**, *10*, 1108–1117.
- (44) Kristensen, A.; Yang, J. K. W.; Bozhevolnyi, S. I.; Link, S.; Nordlander, P.; Halas, N. J.; Mortensen, N. A. Plasmonic colour generation. *Nat. Rev. Mater.* **2017**, *2*, 16088.
- (45) Esposito, M.; Todisco, F.; Bakhti, S.; Passaseo, A.; Tarantini, I.; Cuscunà, M.; Destouches, N.; Tasco, V. Symmetry breaking in oligomer surface plasmon lattice resonances. *Nano Lett.* **2019**, *19*, 1922–1930.
- (46) Baffou, G.; Berto, P.; Bermúdez Ureña, E.; Quidant, R.; Monneret, S.; Polleux, J.; Rigneault, H. Photoinduced heating of nanoparticle arrays. *ACS Nano* **2013**, *7*, 6478–6488.
- (47) Govorov, A. O.; Zhang, W.; Skeini, T.; Richardson, H.; Lee, J.; Kotov, N. A. Gold nanoparticle ensembles as heaters and actuators: Melting and collective plasmon resonances. *Nanoscale Res. Lett.* **2006**, 1, 84.
- (48) Richardson, H. H.; Carlson, M. T.; Tandler, P. J.; Hernandez, P.; Govorov, A. O. Experimental and theoretical studies of light-to-heat conversion and collective heating effects in metal nanoparticle solutions. *Nano Lett.* **2009**, *9*, 1139–1146.
- (49) Baffou, G.; Quidant, R.; Girard, C. Thermoplasmonics modeling: A Green's function approach. *Phys. Rev. B* **2010**, 82, 165424.
- (50) Siahpoush, V.; Ahmadi-kandjani, S.; Nikniazi, A. Effect of plasmonic coupling on photothermal behavior of random nanoparticles. *Opt. Commun.* **2018**, *420*, 52–58.
- (51) Borah, R.; Verbruggen, S. W. Coupled plasmon modes in 2D gold nanoparticle clusters and their effect on local temperature control. *J. Phys. Chem. C* **2019**, *123*, 30594–30603.
- (52) Luo, M.; Zhao, J.; Liu, L.; Antezza, M. Photothermal behavior for two-dimensional nanoparticle ensembles: Multiple scattering and thermal accumulation effects. *Phys. Rev. B* **2022**, *105*, 235431.
- (53) Johnson, P. B.; Christy, R. W. Optical constants of the noble metals. *Phys. Rev. B* **1972**, *6*, 4370–4379.
- (54) García de Abajo, F. J. Multiple scattering of radiation in clusters of dielectrics. *Phys. Rev. B* **1999**, *60*, 6086–6102.
- (55) García de Abajo, F. J. Colloquium: Light scattering by particle and hole arrays. *Rev. Mod. Phys.* **2007**, *79*, 1267–1290.
- (56) Teperik, T. V.; Degiron, A. Design strategies to tailor the narrow plasmon-photonic resonances in arrays of metallic nanoparticles. *Phys. Rev. B* **2012**, *86*, 245425.
- (57) Kolkowski, R.; Koenderink, A. F. Lattice resonances in optical metasurfaces with gain and loss. *Proc. IEEE* **2020**, *108*, 795–818.
- (58) Zundel, L.; Manjavacas, A. Finite-size effects on periodic arrays of nanostructures. *J. Phys.: Photonics* **2019**, *1*, 015004.
- (59) Cuartero-González, A.; Sanders, S.; Zundel, L.; Fernández-Domínguez, A. I.; Manjavacas, A. Super- and subradiant lattice resonances in bipartite nanoparticle arrays. *ACS Nano* **2020**, *14*, 11876.

- (60) García de Abajo, F. J. Interaction of radiation and fast electrons with clusters of dielectrics: A multiple scattering approach. *Phys. Rev. Lett.* **1999**, 82, 2776–2779.
- (61) Zundel, L.; Cuartero-González, A.; Sanders, S.; Fernández-Domínguez, A. I.; Manjavacas, A. Green tensor analysis of lattice resonances in periodic arrays of nanoparticles. *ACS Photonics* **2022**, *9*, 540–550.
- (62) Thongrattanasiri, S.; Koppens, F. H. L.; García de Abajo, F. J. Complete optical absorption in periodically patterned graphene. *Phys. Rev. Lett.* **2012**, *108*, 047401.
- (63) Deop-Ruano, J. R.; Sanders, S.; Alabastri, A.; Kort-Kamp, W. J. M.; Dalvit, D. A. R.; Manjavacas, A. Optical response of periodic arrays of graphene nanodisks. *Phys. Rev. Applied* **2022**, *18*, 044071.
- (64) Zundel, L.; Deop-Ruano, J. R.; Martinez-Herrero, R.; Manjavacas, A. Lattice resonances excited by finite-width light beams. ACS Omega 2022, 7, 31431–31441.
- (65) Baffou, G.; Rigneault, H. Femtosecond-pulsed optical heating of gold nanoparticles. *Phys. Rev. B* **2011**, *84*, 035415.
- (66) Humphrey, A. D.; Barnes, W. L. Plasmonic surface lattice resonances on arrays of different lattice symmetry. *Phys. Rev. B* **2014**, 90, 075404.
- (67) Lunnemann, P.; Koenderink, A. F. Dispersion of guided modes in two-dimensional split ring lattices. *Phys. Rev. B* **2014**, *90*, 245416.
- (68) Humphrey, A. D.; Barnes, W. L. Plasmonic surface lattice resonances in arrays of metallic nanoparticle dimers. *J. Opt.* **2016**, *18*, 035005.
- (69) Li, R.; Bourgeois, M. R.; Cherqui, C.; Guan, J.; Wang, D.; Hu, J.; Schaller, R. D.; Schatz, G. C.; Odom, T. W. Hierarchical hybridization in plasmonic honeycomb lattices. *Nano Lett.* **2019**, *19*, 6435–6441.
- (70) Fradkin, I. M.; Dyakov, S. A.; Gippius, N. A. Nanoparticle lattices with bases: Fourier modal method and dipole approximation. *Phys. Rev. B* **2020**, *102*, 045432.
- (71) Warren, A.; Alkaisi, M. M.; Moore, C. P. Subradiant resonances in Au and Ag bipartite lattices in the visible spectrum. *J. Vac. Sci. Technol.* **2021**, *39*, 063601.
- (72) Novotny, L.; Hecht, B. *Principles of Nano-Optics*; Cambridge University Press: New York, 2006.

# **Supporting Information:**

# **Lattice Resonances for Thermoplasmonics**

Lauren Zundel,<sup>†</sup> Kellen Malone,<sup>†</sup> Luis Cerdán,<sup>‡</sup> Rosario Martínez-Herrero,<sup>¶</sup> and Alejandro Manjavacas\*,<sup>‡</sup>,<sup>†</sup>

†Department of Physics and Astronomy, University of New Mexico, Albuquerque, New Mexico 87106, United States

‡Instituto de Óptica (IO-CSIC), Consejo Superior de Investigaciones Científicas, 28006 Madrid, Spain

¶Departamento de Óptica, Universidad Complutense de Madrid, 28040 Madrid, Spain

E-mail: a.manjavacas@csic.es

### **Table of Contents**

•	Figure S1	• • • •	 	 	 	 P	age S2
•	Figure S2		 	 	 	 P	age S3
•	References		 	 	 	 P	age S4

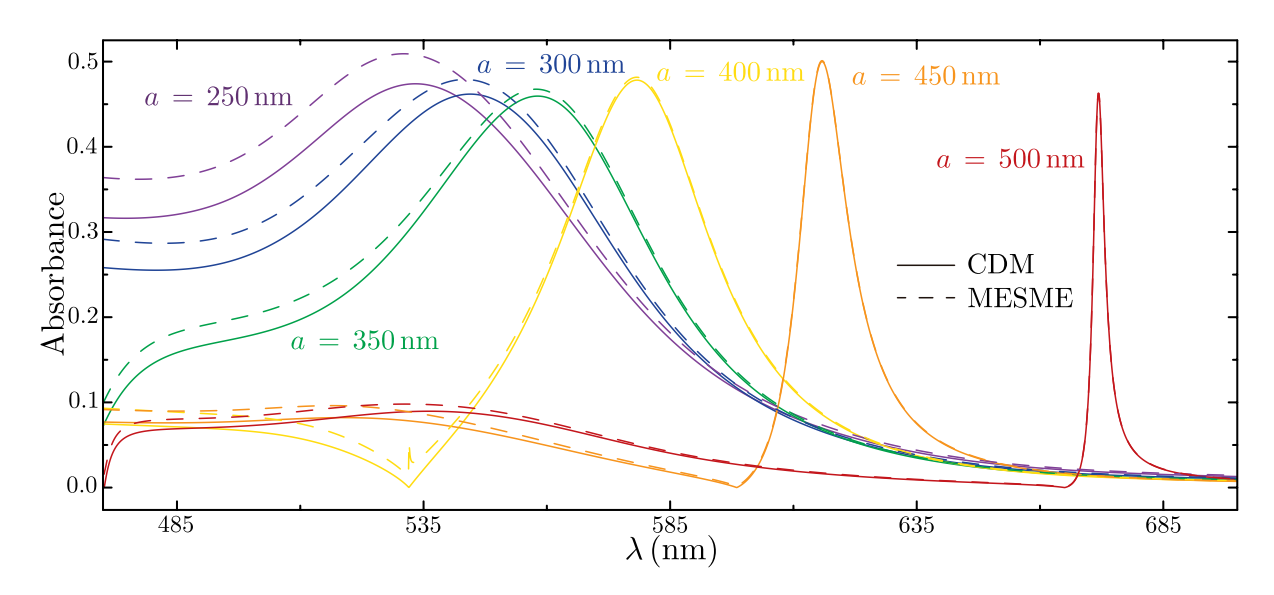


Figure S1: Absorption spectra for arrays of gold nanoparticles with diameter  $D=100\,\mathrm{nm}$  in a uniform refractive index n=1.33. As indicated by the legend, the different colors represent different array periods. The solid curves show the results obtained using the coupled dipole model (CDM), while the dashed ones correspond to rigorous solutions of Maxwell's equations obtained using a multiple elastic scattering of multipole expansions (MESME) approach. S1,S2 In all cases, the arrays are excited by a plane wave.

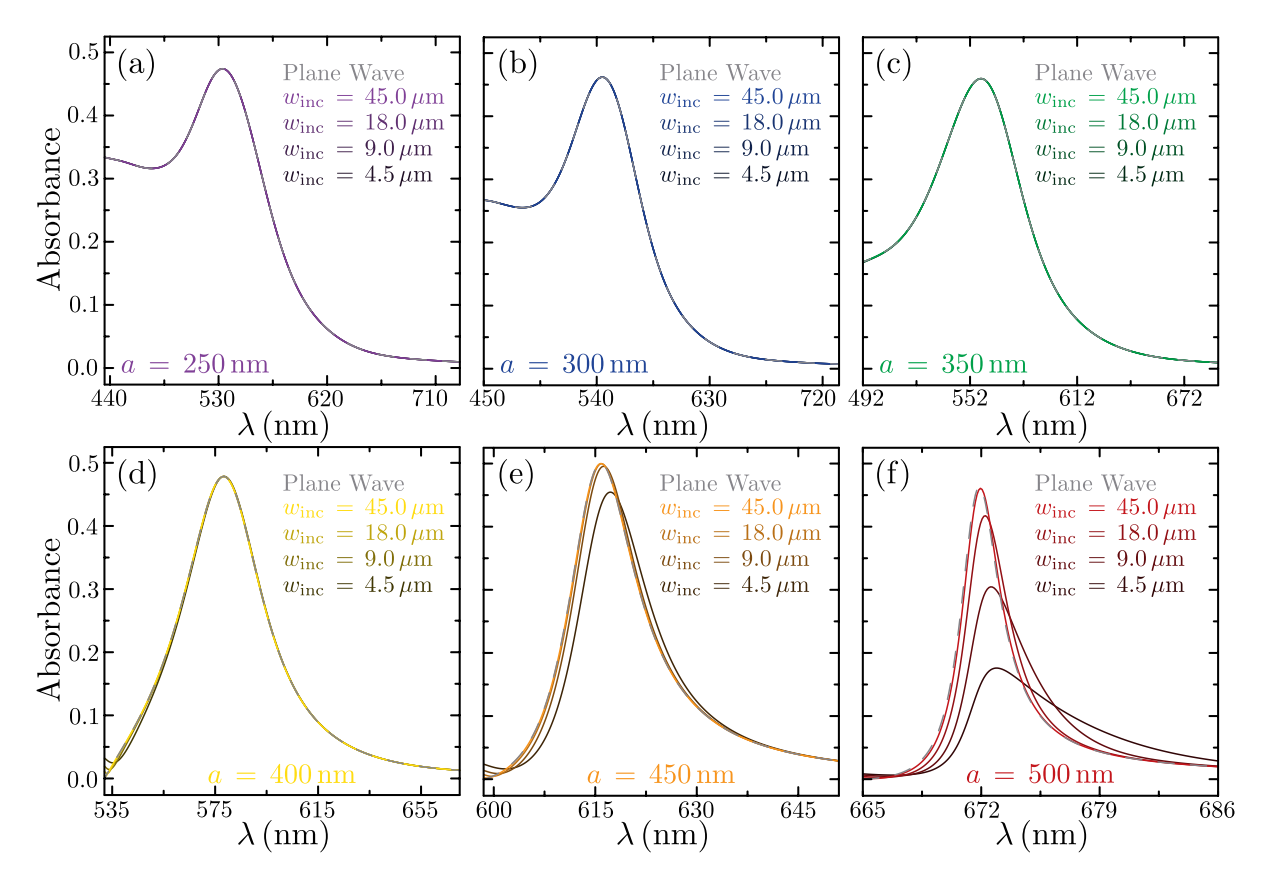


Figure S2: Absorption spectra for arrays of gold nanoparticles with diameter  $D=100\,\mathrm{nm}$  in a uniform refractive index of n=1.33. The arrays have period  $a=250\,\mathrm{nm}$  (a),  $a=300\,\mathrm{nm}$  (b),  $a=350\,\mathrm{nm}$  (c),  $a=400\,\mathrm{nm}$  (d),  $a=450\,\mathrm{nm}$  (e),  $a=500\,\mathrm{nm}$  (f). As indicated by the legends, the arrays are excited by a light beam with  $w_{\mathrm{inc}}$  ranging from  $4.5\,\mu\mathrm{m}$  (darkest curves) to  $45.0\,\mu\mathrm{m}$  (lightest curves). For comparison, we show the response of the arrays to plane-wave excitation using dashed gray curves. As we discuss in the main paper, for the arrays with  $a\leq400\,\mathrm{nm}$ , the absorbance is already indistinguishable from that of the plane-wave for  $w_{\mathrm{inc}}=4.5\,\mu\mathrm{m}$ . On the other hand, for  $a=450\,\mathrm{nm}$  and  $a=500\,\mathrm{nm}$ ,  $w_{\mathrm{inc}}=9.0\,\mu\mathrm{m}$  and  $w_{\mathrm{inc}}=45.0\,\mu\mathrm{m}$ , respectively, are needed to converge to the plane-wave limit.

## References

- (S1) García de Abajo, F. J. Interaction of radiation and fast electrons with clusters of dielectrics: A multiple scattering approach. *Phys. Rev. Lett.* **1999**, *82*, 2776–2779.
- (S2) García de Abajo, F. J. Multiple scattering of radiation in clusters of dielectrics. *Phys. Rev. B* **1999**, *60*, 6086–6102.